Transcriptomic analysis reveals *Streptococcus agalactiae* activation of oncogenic pathways in cervical adenocarcinoma

HONG DUC THI NGUYEN[1], TAN MINH LE[1], DA-RYUNG JUNG[2], YOUNGJAE JO[2], YESEUL CHOI[1], DONGHYEON LEE[1], OLIVE EM LEE[1], JUNGHWAN CHO[3], NORA JEE-YOUNG PARK[3-5], INCHEOL SEO[6], GUN OH CHONG[3,7,8], JAE-HO SHIN[2,9,10] and HYUNG SOO HAN[1,3,11]

[1]Department of Biomedical Science, Graduate School, Kyungpook National University, Daegu 41944, Republic of Korea; [2]Department of Applied Biosciences, Kyungpook National University, Daegu 41566, Republic of Korea; [3]Clinical Omics Institute, Kyungpook National University, Daegu 41405, Republic of Korea; [4]Department of Pathology, School of Medicine, Kyungpook National University, Daegu 41944, Republic of Korea; [5]Department of Pathology, Kyungpook National University Chilgok Hospital, Daegu 41404, Republic of Korea; [6]Department of Immunology, School of Medicine, Kyungpook National University, Daegu 41944, Republic of Korea; [7]Department of Obstetrics and Gynecology, School of Medicine, Kyungpook National University, Daegu 41944, Republic of Korea; [8]Department of Obstetrics and Gynecology, Kyungpook National University Chilgok Hospital, Daegu 41404, Republic of Korea; [9]Department of Integrative Biotechnology, Kyungpook National University, Daegu 41566, Republic of Korea; [10]Next Generation Sequencing Core Facility, Kyungpook National University, Daegu 41566, Republic of Korea; [11]Department of Physiology, School of Medicine, Kyungpook National University, Daegu 41944, Republic of Korea

Received May 20, 2024; Accepted September 6, 2024

DOI: 10.3892/ol.2024.14720

Abstract. Cervical adenocarcinoma (AC), a subtype of uterine cervical cancer (CC), poses a challenge due to its resistance to therapy and poor prognosis compared with squamous cervical carcinoma. *Streptococcus agalactiae* [group B *Streptococcus* (GBS)], a Gram-positive coccus, has been associated with cervical intraepithelial neoplasia in CC. However, the underlying mechanism interaction between GBS and CC, particularly AC, remains elusive. Leveraging The Cancer Genome Atlas public data and time-series transcriptomic data, the present study investigated the interaction between GBS and AC, revealing activation of two pivotal pathways: 'MAPK signaling pathway' and 'mTORC1 signaling'. Western blotting, reverse transcription-quantitative PCR and cell viability assays were performed to validate the activation of these pathways and their role in promoting cancer cell proliferation. Subsequently, the present study evaluated the efficacy of two anticancer drugs targeting these pathways (binimetinib and ridaforolimus) in AC cell treatment. Binimetinib demonstrated a cytostatic effect, while ridaforolimus had a modest impact on HeLa cells after 48 h of treatment, as observed in both cell viability and cytotoxicity assays. The combination of binimetinib and ridaforolimus resulted in a significantly greater cytotoxic effect compared to binimetinib or ridaforolimus monotherapy, although the synergy score indicated an additive effect. In general, the MAPK and mTORC1 signaling pathways were identified as the main pathways associated with GBS and AC cells. The combination of binimetinib and ridaforolimus could be a potential AC treatment.

Correspondence to: Professor Jae-Ho Shin, Department of Applied Biosciences, Kyungpook National University, 80 Daehak-ro, Buk-gu, Daegu 41566, Republic of Korea
E-mail: jhshin@knu.ac.kr

Professor Hyung Soo Han, Department of Physiology, School of Medicine, Kyungpook National University, 680 Gukchaebosang-ro, Jung-gu, Daegu 41944, Republic of Korea
E-mail: hshan@knu.ac.kr

Key words: cervical adenocarcinoma, drug repurposing, signaling pathway, *Streptococcus agalactiae*, transcriptomic time-series analysis

Introduction

Uterine cervical cancer (CC) is the fourth most prevalent cancer type among women globally, underscoring the critical need for ongoing advancements in its management (1). Despite progress in the treatment of CC, the existing therapeutic options have persistent limitations, including side effects and the emergence of drug resistance (2). The histopathological classification of CC identifies two main subtypes: Squamous cell carcinoma (SCC) and adenocarcinoma (AC). While the treatment approach for both subtypes is generally similar, AC is associated with a poorer prognosis than SCC (3). Therefore, addressing the challenges posed by AC remains an essential area for improving overall therapeutic outcomes in CC.

Microbiota are considered to serve a pivotal role in carcinogenesis (4,5). In the context of CC, beyond the well-established risk factor of human papillomavirus, studies have highlighted the contribution of the microbiome to CC development and progression (6,7). It is widely acknowledged that the depletion

of *Lactobacillus* can lead to dysbiosis, characterized by an increase in pathogenic microbial diversity, such as *Atopobium*, *Gardnerella vaginalis*, *Prevotella*, *Sneathia, Streptococcus* and *Megasphaera (*7-9). This microbial imbalance has been associated with damage to the mucus and cytoskeleton structures, alteration of antimicrobial peptides, promotion of proinflammatory cytokine production, and initiation of cervical intraepithelial neoplasia (CIN) (8,10).

Streptococcus, a prominent genus of gram-positive bacteria, has garnered attention in the context of patients with CC (11). Mulato-Briones *et al* (12) identified *Streptococcus* as a predominant bacterium in patients with CC through the culture of cervical exocervix samples. *Streptococcus* is also a potential biomarker for distinguishing between invasive CC and CIN (13). Notably, *Streptococcus agalactiae* [group B *Streptococcus* (GBS)] often colonizes asymptomatically in the female genital tract and can subsequently become a pathogen, leading to severe infections in neonates and adults under certain conditions (14). Previous studies have indicated that GBS stimulates proinflammatory cytokines, including IL-8, IL-1b, IL-6, IL-17 and TNF-α, during its interaction with host epithelial cells (15-18). GBS exhibits a notable capacity to invade cervical epithelial cells and maintain colonization, particularly when compared with vaginal epithelial cells (17). Zhang *et al* (19) revealed that GBS exerts an indirect effect by mediating human papillomavirus infection in patients with CIN. Additionally, GBS has a higher abundance in CIN2 than in CIN1, and has been suggested as a crucial biomarker for predicting the severity of CIN (20). However, to the best of our knowledge, the underlying mechanism of the association between GBS and CC progression, especially AC progression, remains unclear.

Transcriptomics, through differential gene expression and gene ontology analysis, provides a valuable tool for evaluating mechanistic changes during the interaction between host cells and bacteria (21-23). Molecular alterations in cancer-related genes, coupled with the corresponding changes in signaling pathways, guide the development of novel precision medicine treatments for cancer (24). In alignment with this, leveraging transcriptomic analyses also facilitates the exploration of drug repurposing strategies, allowing the identification of existing drugs with potential anticancer properties (25).

In the present study, transcriptomic analyses were performed to elucidate the gene and pathway transcriptome profile of the host CC after GBS infection, particularly for the AC type. Building upon observed RNA sequencing (RNA-seq) data changes, the present approach aimed to connect the findings from the transcriptomic analysis with the potential for drug repurposing. By identifying specific gene expression patterns and altered pathways, this strategy provides a targeted and efficient route for identifying existing drugs that could be repurposed as anticancer therapies, paving the way for further investigation and clinical development.

Materials and methods

Public data acquisition. Expression and clinical data of 304 samples from The Cancer Genome Atlas (TCGA)-CESC were acquired from TCGA Genomic Data Commons portal (https://portal.gdc.cancer.gov/). Metagenomic profiles of the same cohort were sourced from TCGA metagenomic microbiome study (https://ftp.microbio.me/pub/cancer_microbiome_analysis/TCGA). The detailed pipeline for obtaining metagenomic profiles was outlined in a previous study (26). Relative abundance normalization was applied to the metagenomic data, and *Streptococcus* absence was defined as a relative abundance equal to 0.

DESeq2 was employed to investigate differentially expressed genes (DEGs) between *Streptococcus*-present and -absent groups. Significance criteria included an adjusted $P<0.05$ and an absolute $\log_2$-fold change ≥ 0.5 (27).

Weighted gene coexpression network analysis (WGCNA) is a computational method that organizes genes into clusters or modules based on their coexpression patterns across different samples. This approach reveals the complex relationships between genes, providing insights into their roles in biological processes and their connections to disease phenotypes (28,29). In the present study, WGCNA was applied to identify significant genes associated with *Streptococcus* in samples from patients with AC. A soft threshold of $\beta=7$ and a scale-free topology fitting index (R^2) of 0.95 were used for matrix transformation according to the scale-free topological criteria. The modules exhibiting the highest correlation with *Streptococcus* presence were selected. Key genes related to *Streptococcus* in the AC samples were then identified if they met the following criteria: Gene significance (GS) >0.5, module membership (MM) >0.8 and $P<0.05$.

Pathway enrichment analysis was conducted using two web-based tools, including g:Profiler (https://biit.cs.ut.ee/gprofiler/gost; version 2023) (30) and Enrichr (https://maayanlab.cloud/Enrichr/; version June 8, 2023) (31), employing the Kyoto Encyclopedia of Genes and Genomes pathway database (32) and Molecular Signatures Database Hallmark 2020 (33). Statistical significance was established with an adjusted $P<0.1$ and a minimum of four genes per pathway. Significant enriched pathways were visualized using ggplot2 version 3.4.2 (34).

HeLa cell culture. HeLa cells, also known as human AC cell lines (KCLB number 10002; lot no. 59726; passage no. 98; Korean Cell Line Bank; Korean Cell Line Research Foundation), were thawed, cultured and passaged within T75 cell culture flasks using Minimum Essential Medium (Gibco; Thermo Fisher Scientific, Inc.) supplemented with 10% fetal bovine serum (Gibco; Thermo Fisher Scientific, Inc.) in a humidified atmosphere with 5% CO_2 at 37˚C.

Two subculturing instances were conducted to ensure cellular stability for experimentation. Initially, cells were seeded at $5\text{-}6\times10^5$ cells per flask. Media exchange occurred every 2 days or as needed based on cellular conditions, with harvesting conducted once cells achieved 90-95% confluence.

Streptococcus agalactiae exposure experiment using HeLa cells. GBS or *Streptococcus agalactiae* strain NCTC 818 [G19] (13813; American Type Culture Collection) was aerobically grown at 37˚C in Tryptic Soy Broth (Becton, Dickinson and Company) according to the manufacturer's protocol.

HeLa cells were infected with GBS for 0, 2, 6 and 24 h at a multiplicity of infection equal to 100 (GBS:cell=100:1). Right before the experiment, GBS in the bacterial medium was precipitated and resuspended in human medium

(Minimum Essential Medium supplemented with 10% fetal bovine serum), ensuring the concentration remained consistent with the 100:1 ratio. For the control group, human medium without bacteria was administered. Following this, the flasks were incubated for 0 (baseline), 2, 6 and 24 h in a humidified atmosphere with 5% CO_2 at 37˚C.

All experiments were conducted in triplicate.

RNA isolation and sequencing. Total RNA was isolated from HeLa cells cocultured with GBS using the RNeasy Mini Kit (74104; Qiagen GmbH) according to the manufacturer's protocol. Ribosomal RNA depletion was performed using the MGIEasy rRNA Depletion Kit (1000005953; MGI Tech Co., Ltd) and library preparation was performed using the MGIEasy RNA Directional Library Prep Set (1000006386; MGI Tech Co., Ltd.). The final library concentration was 113 nM. Sample quantification was performed using the Qubit ssDNA Assay Kit (Q10212; Invitrogen; Thermo Fisher Scientific, Inc.) and the Invitrogen Qubit Fluorometer (Q33216; Thermo Fisher Scientific, Inc.). Sample quality was assessed using an Agilent 2100 Bioanalyzer (G2939AA; Agilent Technologies, Inc.). Sequencing was conducted on the DNBSEQ-G400 sequencer (MGI Tech Co., Ltd.) using the DNBSEQ-G400RS-High throughput sequencing FCL PE100 kit (1000016949; MGI Tech Co., Ltd.), generating 100-bp paired-end reads.

FASTQ files from the sequencer underwent quality assessment using FASTQC v0.12.1 and Multiqc version 1.24.1 (35,36). Cutadapt version 4.9 was employed to eliminate low-quality reads and sequencing adapters (37). The alignment and quantification of RNA-seq data were performed using STAR version 2.7.11b (38). Detailed information on sequenced and mapped samples can be found in Table SI.

Time-series transcriptomic analysis of GBS-HeLa cell interactions. TimeSeriesAnalysis (TiSA) is a tool including analysis and visualization packages for RNA-seq and microarrays. It facilitates the extraction of significant genes from time series transcriptomic data by assessing differential gene expression along both condition and temporal axes (39).

In the present study, TiSA was used to identify significant genes meeting the criteria of an absolute $\log_2$-fold change ≥1 and an adjusted P<0.05 from longitudinal transcriptomic data, elucidating the interaction between HeLa cells and GBS.

A principal component analysis (PCA) plot was generated using the first and second principal components to visualize the differences between control and GBS-exposed HeLa cell groups at various time points. This was conducted using the plot_PCA_TS() function from the TiSA package. The partitioning algorithm based on recursive thresholding (PART) from the clusterGenomics R package, version 1.0 (40), was applied for clustering. DEGs and clusters were visualized using heatmaps, created with the ComplexHeatmap package version 2.8.0 (http://www.bioconductor.org/packages/devel/bioc/html/ComplexHeatmap.html). To elucidate the biological meaning of the clusters, Enrichr and g:Profiler were used, with the criteria as aforementioned.

Reverse transcription-quantitative PCR (RT-qPCR). Total RNA was extracted from GBS-exposed HeLa cells after 24 h to validate the mRNA expression of the genes belonging to the MAPK pathway [fibroblast growth factor 21 (FGF21), nerve growth factor (NGF), IL1A and IL1B] and mTORC1 pathway [DNA damage inducible transcript 3 (DDIT3), cystathionine γ-lyase (CTH), asparagine synthetase (glutamine-hydrolyzing) (ASNS) and nuclear protein 1 (NUPR1) using the RNeasy Mini Kit (74104; Qiagen GmbH). RT-qPCR was performed using a one-step TOPreal™ SYBR Green RT-qPCR Kit (cat. no. RT432S; Enzynomics Co., Ltd.) on a Thermal Cycler Dice Real Time System TP800 (Takara Bio, Inc.). This one-step kit combines high-yield TOPscript reverse transcriptase (cat. no. RT002; Enzynomics Co., Ltd.) with chemically modified Taq polymerases. According to the manufacturer's instructions, reverse transcription was performed at 50˚C for 30 min, and the thermocycling conditions were as follows: Initial denaturation at 95˚C for 10 min, followed by 45 cycles of denaturation at 95˚C for 5 sec, and annealing and elongation at 60˚C for 30 sec. The primer sequences utilized are presented in Table SII.

All reactions were performed in triplicate. The relative expression levels of the target genes were normalized to the reference gene (GAPDH) using the ΔCq method. Fold changes in gene expression were calculated using the $2^{-\Delta\Delta Cq}$ method, with the control sample serving as the calibrator (41).

Western blotting. To validate the activation of significantly enriched pathways in HeLa cells after 24 h of exposure to GBS, western blotting was performed. HeLa cells were co-cultured with GBS for 24 h, washed with cold PBS and lysed using cold M-PER™ Mammalian Protein Extraction Reagent containing 0.2% Halt™ Protease Inhibitor Cocktail (Thermo Fisher Scientific, Inc.). Tumor cell lysates (20 μg/lane; protein concentration quantified using a Bradford assay) were loaded onto a 4-20% Mini-PROTEAN TGX precast gel (Bio-Rad Laboratories, Inc.) and electrophoresed for 10 min at 80 V, followed by 60-90 min at 120 V. The proteins were transferred to PVDF membranes for 45 min at 12 V using the semi-dry blotting system (ATTO Corporation). After blocking with 5% skim milk for 1 h at room temperature, the membranes were incubated overnight at 4˚C with the following primary antibodies: ERK1/2, phosphorylated ERK1/2 (p-ERK1/2), phosphorylated mTOR at Ser2448 (p-mTOR), p38, phosphorylated p38 (p-p38), panAKT (each at a dilution of 1:1,000), mTOR (dilution, 1:2,000), phosphorylated AKT at Ser473 (p-AKT) and Ki67 (each at a dilution of 1:5,000). Detailed information about the antibodies is provided in Table SIII.

Following incubation, the membranes were treated for 1 h at room temperature with anti-rabbit IgG HRP-linked antibody and anti-mouse IgG HRP for β-actin antibody at a dilution of 1:5,000. The membranes were washed three times with 1X TBS with 0.1% Tween-20 for 10 min. The PVDF membranes were then processed with a PicoEPD Western Blot Detection kit (EBP1073; ELPIS-Biotech, Inc.). The chemiluminescence images were captured using the Amersham Imager 600 (GE Healthcare), and the resulting bands were semi-quantified to determine relative protein levels using ImageJ software version 1.54 (National Institutes of Health). The experiments were conducted in triplicate for both control and treatment groups.

Therapeutic agents. Candidate therapeutic agents were selected through a drug repurposing approach. One valuable tool in drug repurposing is the Connectivity Map (CMap) tool (42). CMap is a powerful platform for unraveling connections among drugs, genes and diseases. The fundamental principle involves comparing the gene expression profiles induced by a specific drug with those associated with particular diseases (42).

Genes from TiSA clusters of interest were uploaded to the CMap web-based tool version 1.1.1.43 (https://clue.io/). Potential anticancer drugs were identified based on their tau score, which is converted from normalized connectivity scores, comparing them with values of that disease for all the drugs in the reference database (43,44). Tau scores exceeding 90 or below-90 between two signatures indicate strong connectivity. A negative connectivity signifies the reversal of the disease signature by the drug (43).

Binimetinib (MEK162) was purchased from Selleck Chemicals (cat. no. S7007). A 10 mM stock solution was generated in DMSO and stored at -20˚C.

Ridaforolimus (deforolimus; cat. no. HY-50908; MedChemExpress) was prepared as 10 mM stock solutions with DMSO and stored at -20˚C.

Specially tailored working solutions of these drugs were prepared for immediate use. In the case of monotherapy, binimetinib and ridaforolimus were serially diluted to concentrations of 0.625, 1.25, 2.5, 5, 10, 15 and 20 μM. For combination therapy of binimetinib and ridaforolimus, a 1:1 ratio of the drugs was applied, with serial dilutions of 1.25, 2.5, 5, 10, 15 and 20 μM used. For all treatments the cells were incubated at 37˚C with 5% CO_2. Each experiment was conducted in triplicate.

Trypan blue assay. A trypan blue assay was utilized to evaluate the viability of HeLa cells following exposure to GBS or therapeutic agents. After washing with PBS, adherent cells in a 90-mm plate were dissociated using 2 ml of 0.25% trypsin-EDTA for 2 min at room temperature. The cells were then resuspended in 8 ml cell culture medium. A portion of this cell suspension was mixed with an equal volume of 0.4% trypan blue (Gibco; Thermo Fisher Scientific, Inc.) for 2 min at room temperature. The number of viable and non-viable cells was counted in triplicate using a hemocytometer.

MTS assay. After reaching confluence in a T75 flask, HeLa cells were subcultured into 96-well plates at a concentration of $2x10^4$ cells/100 μl. Following a 24-h incubation period, binimetinib and/or ridaforolimus were added into each well using serial dilutions of 1.25, 2.5, 5, 10, 15 and 20 μM.

Subsequently, the cells were incubated at 37˚C with 5% CO_2 for either 24 or 48 h. Afterwards, 20 μl CellTiter 96® AQueous One Solution (G3582; Promega Corporation) reagent was added to each well. The plate underwent an additional 4-h incubation at 37˚C with 5% CO_2, and the absorbance at 490 nm was measured using a microplate reader (Multiskan™ FC; Thermo Fisher Scientific, Inc.).

The absorbance intensity at 490 nm for both the control and treatment groups was normalized to the absorbance of the background. Subsequently, cell viability percentages for different treatment groups were calculated using the following formula: % viability=adjusted optical density $(OD)_{sample}$/mean (adjusted $OD_{control}$), where adjusted OD_{sample}=OD_{sample}-mean ($OD_{background}$), and adjusted $OD_{control}$=$OD_{control}$-mean ($OD_{background}$).

Cell apoptosis assay. To measure the induction of apoptosis, $5x10^5$ HeLa cells were plated in 90-mm plates and allowed to adhere and proliferate for 48 h. Cells were then treated with either 15 μM binimetinib, 20 μM ridaforolimus, a combination of both (5 μM binimetinib + 5 μM ridaforolimus) or DMSO (vehicle treatment) as a control at 37˚C with 5% CO_2.

After 48 h, cells were harvested and transferred into tubes at a concentration of $5x10^5$ cells/ml. Cell death was assessed using an annexin V-FITC apoptosis detection kit (ab14085; Abcam) with 5 μl annexin V-FITC and 5 μl PI, followed by a 5-min incubation at room temperature in the dark. The apoptosis assay data were obtained using a BD FACSCalibur flow cytometer (BD Biosciences). The graph showing the percentages of apoptotic and necrotic cells was created using the Floreada tool (https://floreada.io; WASM version SIMD).

Dose-response curve and synergy scores. To estimate the efficacy of anticancer drugs, the dose-response curve R package version 3.0.1 was used to determine the IC_{50} (45). The IC_{50} values represent the concentrations of each drug required to achieve a 50% inhibition of cancer cell viability.

To predict the combination (binimetinib and ridaforolimus) effect, the synergy score was calculated using the SynergyFinder R package version 3.8.2 (46). If the synergy score is between -10 and 10, the effect of the combination of the two drugs is additive, if the score is >10, the effect is synergistic, and if the score is <-10, the combination is considered antagonistic (46,47).

Effect of therapeutic agents on GBS-exposed HeLa cells. To evaluate the effect of therapeutic agents on GBS-exposed HeLa cells and to compare these effects with those on HeLa cells not exposed to GBS, GBS and HeLa cells were co-cultured at a ratio of 100:1 in a humidified atmosphere with 5% CO_2 at 37˚C for 6 h. Following this exposure, the GBS-exposed HeLa cells were treated with 15 μM binimetinib, 20 μM ridaforolimus, a combination of both (5 μM binimetinib + 5 μM ridaforolimus) or DMSO as a control at 37˚C with 5% CO_2. The number of dead and viable cells after 24 h of treatment was measured using a trypan blue assay in triplicate as aforementioned.

Statistical analysis. To compare two groups, an unpaired Student's t-test was performed. For analyses involving multiple groups, one-way ANOVA followed by post hoc testing using the Holm-Bonferroni correction method was performed (48). All statistical analyses were performed using the stats package version 4.3.3 (https://search.r-project.org/R/refmans/stats/html/00Index.html) in R version 4.3.3 (https://www.R-project.org/). The results were visualized using the ggplot2 package version 3.4.2 (34) and ggpubr package version 0.6.0 (https://github.com/kassambara/ggpubr). Analyses were based on three experimental repeats. In the plots, error bars were included to represent the dispersion of the variable (standard deviation). $P<0.05$ was considered to indicate a statistically significant difference.

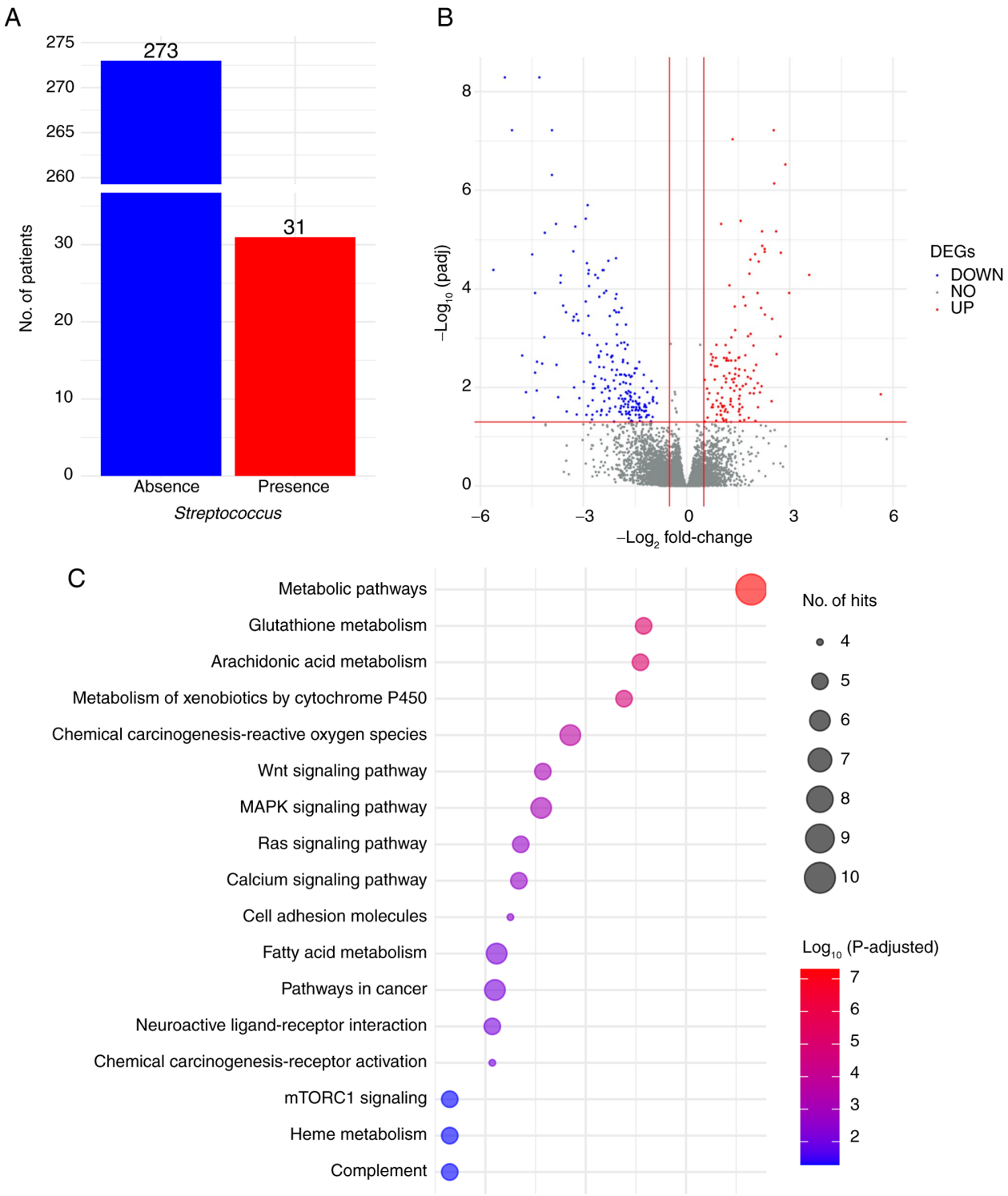

Figure 1. Gene expression and pathway profiles of *Streptococcus*-associated CC using The Cancer Genome Atlas-CESC public data. (A) Distribution of *Streptococcus*-present and -absent cases. (B) DEG profiles between *Streptococcus*-present and -absent CC groups, with red and blue indicating upregulated and downregulated genes, and grey representing non-significantly DEGs. (C) Pathway profiles of upregulated DEGs. CC, cervical cancer; DEG, differentially expressed gene; padj, adjusted P-value.

Results

Gene expression and pathway profiles of Streptococcus-associated CC using TCGA-CESC public data. To investigate the relationship between *Streptococcus* and CC, a cohort of 304 TCGA CC cases, including transcriptomic data and *Streptococcus* abundance profiles, were analyzed (Table SIV). As shown in Fig. 1A, 31 cases (10.2%) exhibited the presence of *Streptococcus*.

DEG profiles (Fig. 1B) revealed 128 upregulated and 209 downregulated DEGs identified using DESeq2 (Table SV). Pathway enrichment analysis, conducted using the web-based tools g:Profiler and Enrichr, of the list of 128 upregulated DEGs, highlighted statistically and biologically significant

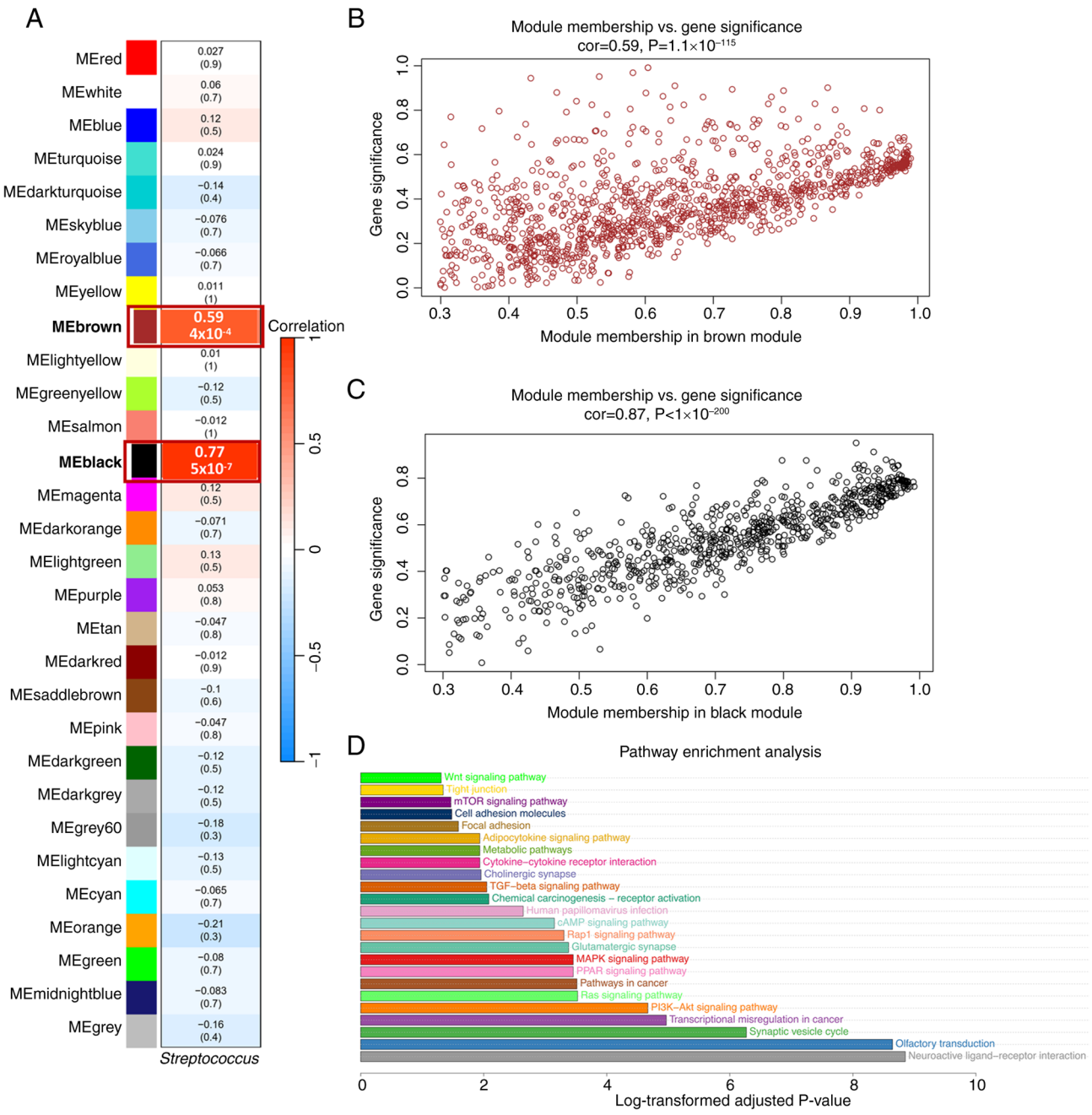

Figure 2. *Streptococcus*-related transcriptomic and pathway profiles in 31 patients with cervical adenocarcinoma from The Cancer Genome Atlas analyzed using weighted gene co-expression network analysis. (A) Heatmap of the correlation between *Streptococcus* abundance and module eigengenes. Each row corresponds to a module, and the color gradient indicates correlation coefficients, with blue representing negative correlations and red representing positive correlations. Corresponding P-values are displayed in brackets. (B) Scatter plot of the correlation between MM of the brown module and GS for *Streptococcus* abundance. (C) Scatter plot of correlation between MM of the black module and GS for *Streptococcus* abundance. (D) Bar plot showing results of pathway enrichment analysis for significant genes from the brown and black modules with GS >0.5, MM >0.8 and P<0.05. AMPK, AMP-activated protein kinase; GS, gene significance; ME, module eigengenes; MM, module membership; PPAR, peroxisome proliferator-activated receptor.

pathways associated with cancer, including 'MAPK signaling pathway', 'mTORC1 signaling', 'Ras signaling pathway' and 'Wnt signaling pathway', as well as metabolism pathways such as 'metabolism of xenobiotics by cytochrome P450', 'fatty acid metabolism', 'glutathione metabolism' and 'arachidonic acid metabolism' (Fig. 1C; Table SVI).

To further explore the specificity of the relationship between *Streptococcus* and AC, 31 patients with AC from a cohort of 304 patients with CC in TCGA were analyzed. Among them, 3 patients with AC exhibited the presence of *Streptococcus* (Table SIV). Using the WGCNA tool, two significant key modules with high correlation values, r=0.77 (P=5x10^{-7}) for the black module and r=0.59 (P=4x10^{-4}) for the brown module, were identified (Fig. 2A-C; Tables SVII and SVIII).

A total of 500 key genes related to *Streptococcus* were selected from the two key modules based on the following criteria: GS >0.5, MM >0.8 and P<0.05. Pathway enrichment analysis showed that these genes were involved multiple oncogenic pathways, including 'MAPK signaling pathway', 'mTOR signaling pathway', 'PI3K-AKT signaling pathway', 'TGF-beta

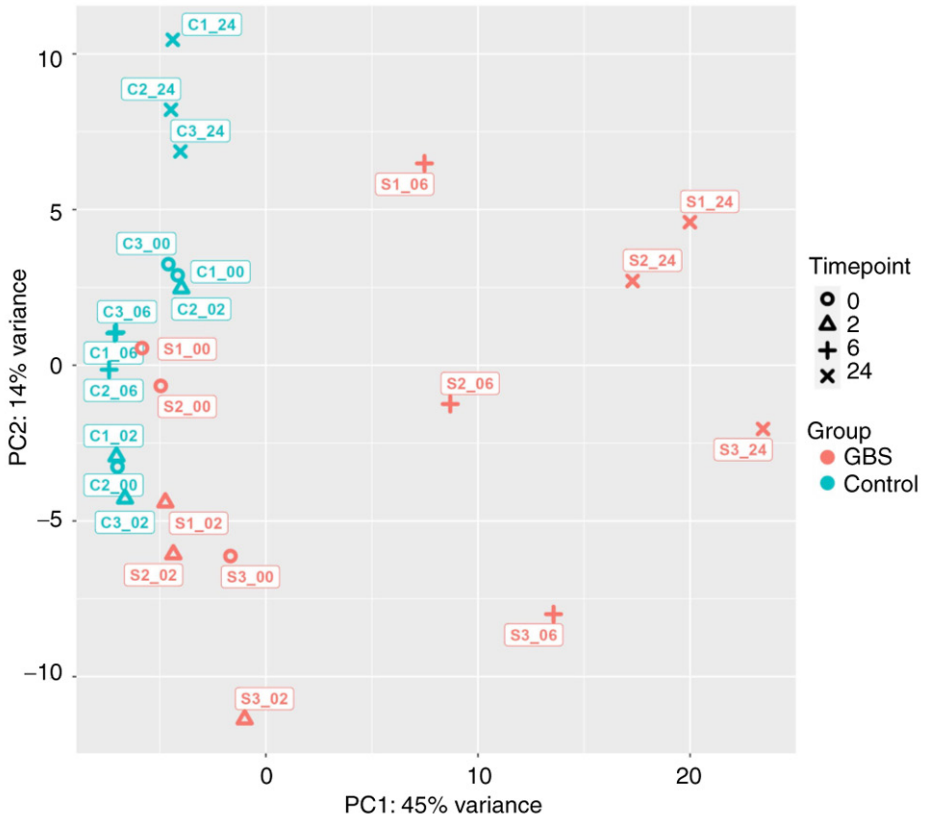

Figure 3. PCA plot. The PCA plot illustrates each sample from two groups: The GBS group and the control group. In the plot, HeLa cells exposed to GBS are represented in red for the time points 0, 2, 6 and 24 h. The control group is denoted by the blue color. Additionally, each time point is distinguished by specific shapes: Circles for 0 h, triangles for 2 h, crosses for 6 h and multiplication signs for 24 h. GBS, group B *Streptococcus*; PCA, principal component analysis.

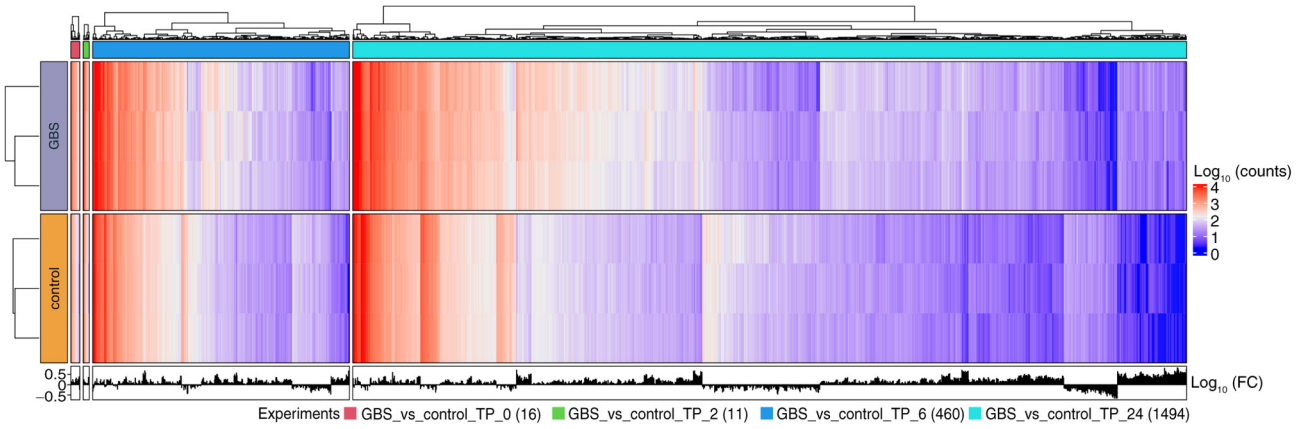

Figure 4. Heatmap of conditional and temporal differentially expressed genes. The rows indicate the condition, and the columns indicate the genes. The conditions are divided into exposure to GBS in purple and the control group in orange. The genes are grouped according to the time points: 0 h in red, 2 h in green, 6 h in blue and 24 h in cyan. FC, fold change; GBS, group B *Streptococcus*; TP, timepoint.

signaling pathway' and 'Ras signaling pathway' (Fig. 2D; Table SIX).

Time-series transcriptomic analysis of GBS-HeLa cell interaction. To further enhance the insights gained from TCGA-CESC data, a time-series experiment was performed to investigate HeLa cell-GBS interactions. Briefly, HeLa cells were infected with GBS for 0, 2, 6 and 24 h, with corresponding control groups treated solely with bacteria-free human medium. Subsequently, the transcriptomic data generated from this experiment were analyzed using the TiSA package.

PCA plot, and DEGs between conditional and temporal groups. The time series PCA plot demonstrated a clear separation between the GBS-exposed HeLa cell groups at 6 and 24 h and the other groups. PC1, representing variability over time, and PC2, representing differences between groups, were utilized for this analysis. As shown in Fig. 3, the dominance of PC1, accounting for 45% of the variation, while PC2

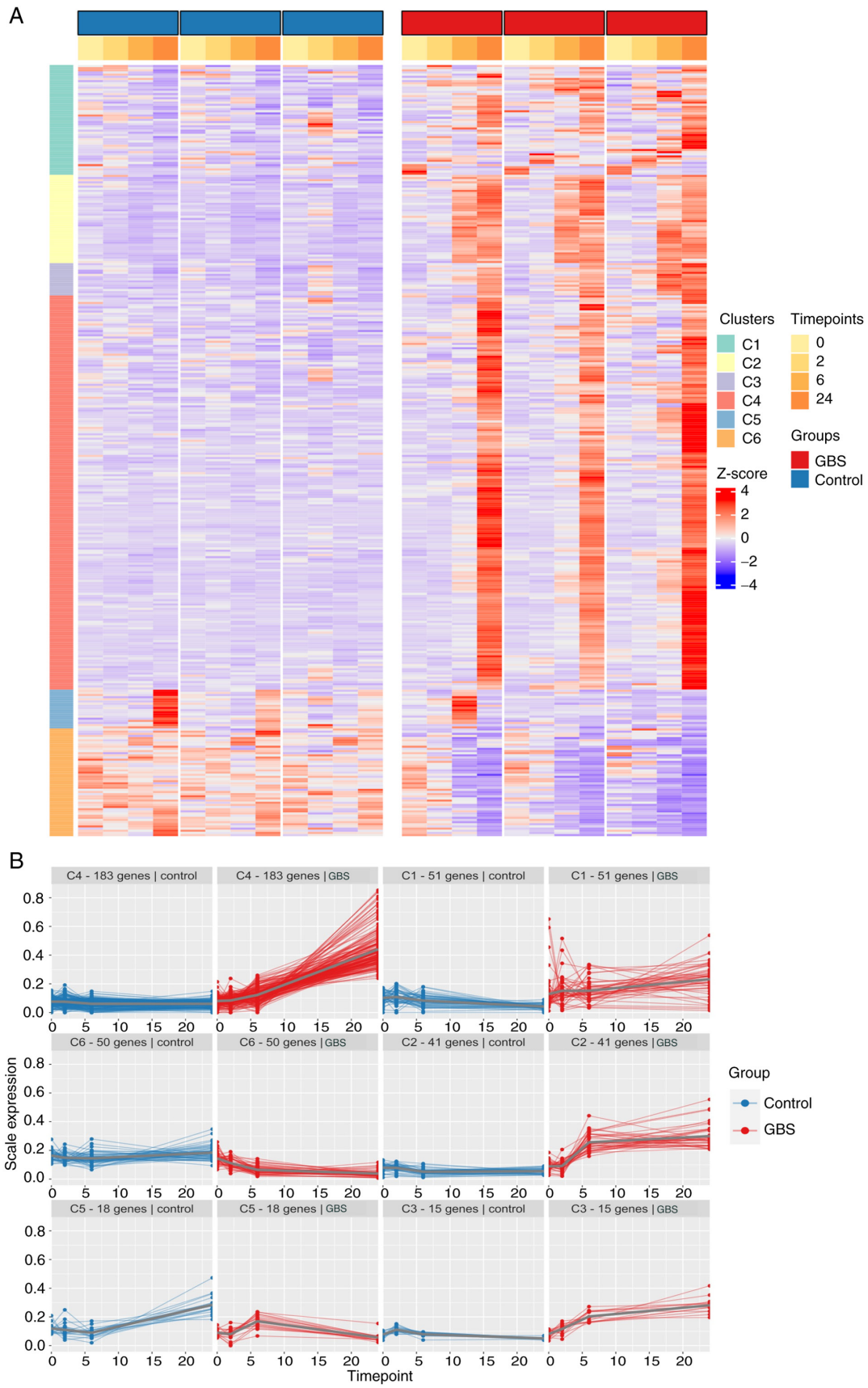

Figure 5. Clustering results. (A) Heatmap of partitioning algorithm based on recursive thresholding clustering including 6 clusters with different colors, following exposure of HeLa cells to GBS across different time points. Condition groups are represented at the top, with the control group indicated in blue and the GBS group indicated in red. The yellow and orange bar colors represent the time points below the condition groups. (B) Gene expression trajectory plot for six clusters identified from time series analysis comparing between GBS exposure and control groups. Each plot shows the average expression trend for all genes in each cluster across the time points, with the x-axis representing time points (h after exposure) and the y-axis showing normalized gene expression levels. Red curves represent the gene expression trajectories in GBS-exposed HeLa cells, and blue curves represent the control group. GBS, group B *Streptococcus*.

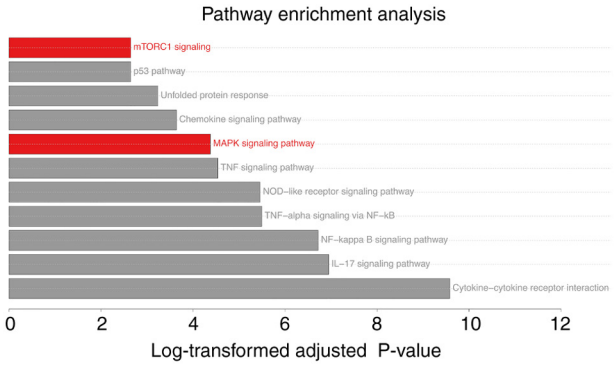

Figure 6. Enriched pathways of cluster 2. The 'MAPK signaling pathway' and 'mTORC1 signaling' (shown in red) were identified in both the time-series analysis and the public data analysis. NOD, nucleotide-binding oligomerization domain.

accounted for 14%, indicated that the variation over time was more pronounced than the variation between groups, which was especially evident after 6 h. Notably, the groups associated with GBS stimulation at 6 and 24 h exhibited a distinct separation from the other groups.

The conditional differential gene expression analysis for four-time points is presented in Fig. 4. The number of DEGs markedly increased after 6 h of exposure. Specifically, there were 16, 11, 460 and 1,494 DEGs after 0, 2, 6 and 24 h of exposure, respectively.

Clustering analysis. All DEGs identified from the conditional differential gene expression analysis, totaling 1,981 genes, were utilized for PART clustering, resulting in six clusters, as shown in Fig. 5A and Table SX. Genes in clusters 1, 2, 3 and 4 showed an upward trajectory between 6 and 24 h, while genes in cluster 6 decreased during the same period. Cluster 5 exhibited mixed expression patterns (Fig. 5B).

Pathway enrichment analysis. Functional analysis of each cluster was performed using Enrichr and g:Profiler. Cluster 2 exhibited the most significant pathways, encompassing both oncogenic pathways ('MAPK signaling pathway', 'mTORC1 signaling' and 'p53 pathway') and immune response pathways ('TNF signaling pathway', 'NF-kappa B signaling pathway', 'IL-17 signaling pathway' and 'NOD-like receptor signaling pathway') (Table SXI).

The pathway enrichment analyses revealed the upregulation of 'MAPK signaling pathway' and 'mTORC1 signaling' in the HeLa cells-GBS exposure experiment (Fig. 6) and the TCGA-CESC public data (Fig. 1C). Additionally, activation of the 'MAPK signaling pathway' and 'mTOR signaling pathway' was observed in the group of 3 patients with AC with *Streptococcus* presence (Fig. 2D). These findings suggested that the MAPK and mTORC1 pathways may serve significant roles in AC associated with GBS.

Validation of MAPK and mTORC1 signaling pathway activation after GBS exposure. To validate the activation of the MAPK and mTORC1 pathways, the upregulated expression of genes associated with the MAPK pathway (FGF21, NGF, IL1A and IL1B) and the mTORC1 pathway (DDIT3, CTH, ASNS and NUPR1) from cluster 2 was first confirmed using RT-qPCR. As shown in Fig. 7C, most of these genes exhibited higher expression levels in HeLa cells exposed to GBS for 24 h compared with control cells, with the exception of NGF. This discrepancy may arise from differences in sensitivity or specificity between RNA-seq and RT-qPCR methods. Overall, the RT-qPCR results support the activation of the MAPK and mTORC1 pathways in response to GBS exposure.

Western blot analysis revealed a significant increase in the ratios of p-ERK1/2 to total (t-)ERK1/2, p-AKT to t-AKT and p-mTOR to t-mTOR in HeLa cells exposed to GBS for 24 h compared with control cells. Although the ratio of p-p38 to t-p38 was higher in the treated HeLa cells than in the control group, the difference was not statistically significant (Fig. 7D). The elevated phosphorylation of ERK1/2 indicated enhanced MAPK pathway activity, while the upregulation of p-AKT and p-mTOR suggested activation of the mTORC1 pathway, further supporting the involvement of these signaling cascades in the cellular response to GBS exposure.

Additionally, the trypan blue assay demonstrated a decrease in viable HeLa cell numbers at 6 h compared with control cells, followed by a significant increase in HeLa cell numbers, reaching levels similar to control cells by 24 h (Fig. 7A). This cell proliferation phenomenon was confirmed by examining the expression of Ki67, a well-known cell proliferation marker. The highest Ki67 expression was observed after 6 h of exposure and the expression was still increased at 24 h compared with that in the control group (Fig. 7B). This pattern may reflect cancer cell proliferation influenced by MAPK and mTORC1 pathway activity after 6 h of exposure to GBS.

Overall, transcriptomic analysis using public data, time-series co-culture experiments, and validation through RT-qPCR and western blotting assays underscored the pivotal role of the MAPK and mTORC1 signaling pathways. These promising results led to the hypothesis that inhibiting these pathways could be effective in treating AC.

Therapeutic agent selection. To further investigate candidate drugs targeting the MAPK and mTORC1 signaling pathways, the list of genes from cluster 2 was uploaded to the CMap web-based tool. Ridaforolimus (or deforolimus) was chosen as the mTOR inhibitor due to its highest negative range score (Table SXII). Notably, to the best of our knowledge, it has not been extensively studied in the context of AC or HeLa cells.

While CMap suggested several anticancer drugs to inhibit the MAPK pathway, these drugs were previously investigated in HeLa cells (49-51). Therefore, binimetinib, a MEK inhibitor that has shown efficacy in other cancer types (52,53) but has not yet been explored in AC, was selected for further evaluation in the present study.

Evaluating the effects of therapeutic agents on HeLa cells

Binimetinib. Although the viability of HeLa cells only notably decreased after 24 h of exposure to doses >20 μM compared with the control group, a significant reduction in cell viability was observed across all binimetinib concentrations (1.25-20 μM) following 48 h of treatment (Figs. 8A and S1). The IC_{50} was determined to be 14.40±2.55 μM (Fig. 8A).

For the apoptosis assay, binimetinib was administered at a concentration of 15 μM, corresponding to the IC_{50} value observed in the MTS assay. The apoptotic effect after 48 h

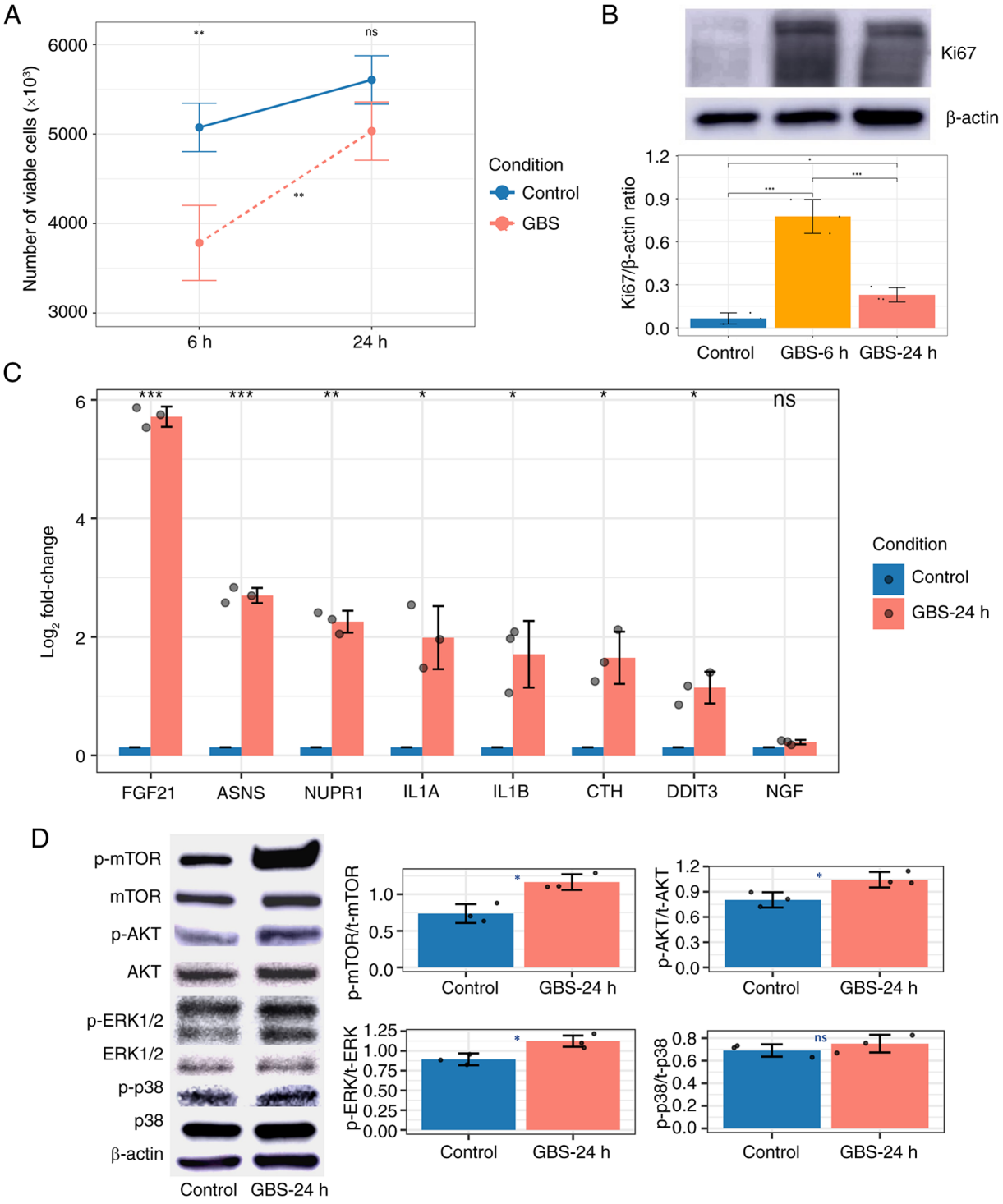

Figure 7. Effects of GBS on HeLa cells. (A) Line graph showing HeLa cell proliferation after 6 and 24 h of GBS exposure, with comparisons with control cells and between two time points, as measured by the trypan blue assay. (B) Western blot analysis and corresponding bar plot showing Ki67 expression in HeLa cells at 6 and 24 h post-GBS exposure. (C) Bar plot showing the logarithm fold changes in the expression of eight targeted genes as determined by reverse transcription-quantitative PCR. (D) Western blot analysis and corresponding bar plots showing the levels of proteins in HeLa cells 24 h after GBS exposure. Blue, orange and red indicate the control group, the 6 and 24-h GBS-treated groups, respectively. *P<0.05, **P<0.01, ***P<0.001. GBS, group B *Streptococcus*; ns, not significant; p-, phosphorylated; t-, total.

of binimetinib treatment was higher than that observed in the control group; nevertheless, no significant difference was detected between the two groups (Figs. 9 and S2B).

Ridaforolimus. The MTS assay revealed minimal inhibitory effects of ridaforolimus on HeLa cell proliferation. No significant reduction in cell viability was observed after treatment with ridaforolimus for 24 and 48 h (Figs. 8B and S3). The IC_{50} of 59.61±10.01 μM further supported this observation (Fig. 8B).

Based on this finding, the highest concentration of ridaforolimus (20 μM) was used for the apoptosis assay. This dose exhibited a weak cytotoxic effect (Figs. 9 and S2C).

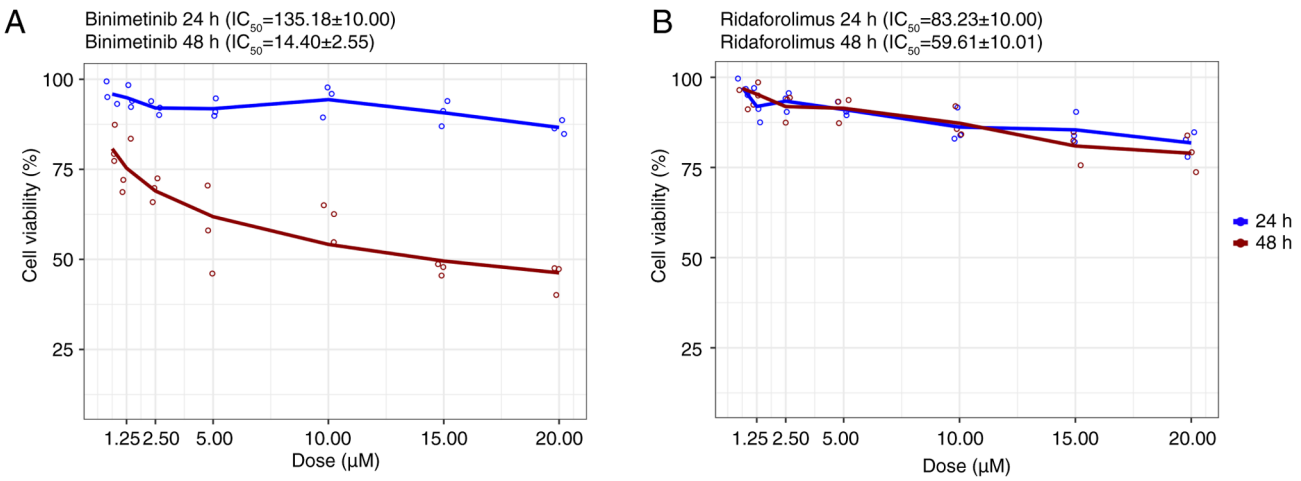

Figure 8. MTS assay results for monotherapies in HeLa cells. (A) Binimetinib and (B) ridaforolimus. Blue and dark red represent drug exposure durations of 24 and 48 h, respectively.

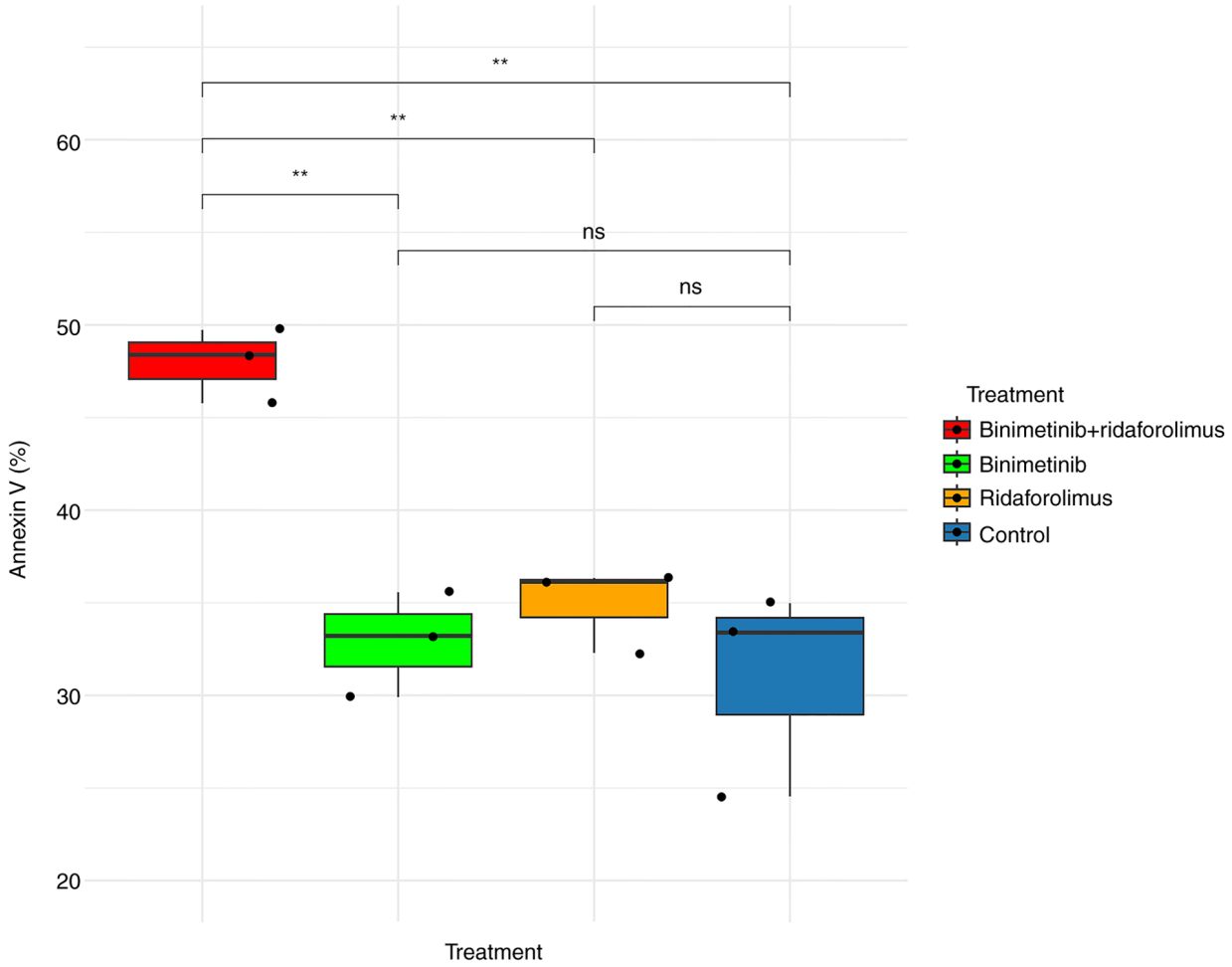

Figure 9. Apoptosis assay results for therapeutic agents in HeLa cells. Green, orange, red and blue represent the binimetinib, ridaforolimus, combination (binimetinib + ridaforolimus) and control groups, respectively. **P<0.01. ns, not significant.

Combination effect of binimetinib and ridaforolimus on HeLa cells. A 1:1 ratio of binimetinib and ridaforolimus was administered to assess the impact of combination therapy. SynergyFinder was used to predict potential synergy, and the results suggested that this combination may exhibit an additive effect, as indicated by a Loewe synergy score of ~4.31, with statistical significance at P<0.05 (Fig. 10). Compared with ridaforolimus alone, the combination of binimetinib and ridaforolimus showed significantly greater inhibition of cell viability in the MTS assay. However, significant differences

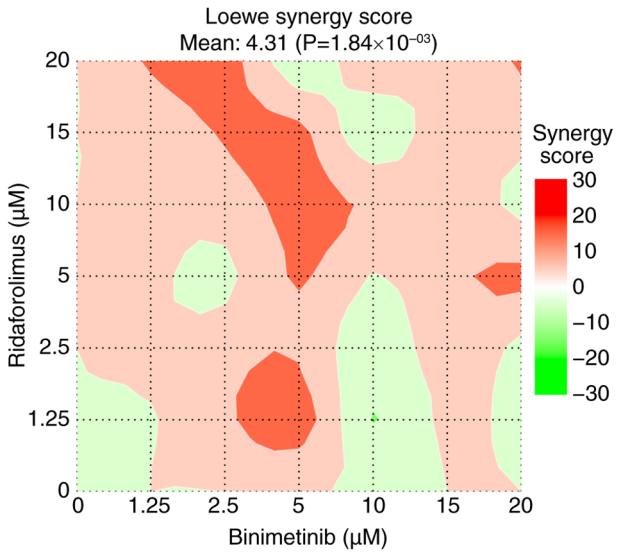

Figure 10. Contour plot. Loewe synergy score of the binimetinib and ridaforolimus combination in HeLa cells after 48 h.

between the combination and binimetinib alone were observed only at concentrations of 10 and 20 μM (Fig. 11).

For the apoptosis assay, 5 μM binimetinib and 5 μM ridaforolimus were used, as this combination effectively reduced cell viability by 50% as indicated by the MTS assay. Although the predictive tool suggested an additive effect, the combination therapy induced notable cytotoxic effects, as evidenced by the highest percentage of annexin V observed 48 h after treatment in the apoptosis assay (Figs. 9 and S2D).

Furthermore, the IC_{50} of this combination, calculated using the dose-response curve package, was determined to be 6.67±0.45 μM for each drug (Fig. S4). In practical terms, this translates to a dose reduction of 2.16 times for binimetinib and 8.94 times for ridaforolimus to reach the IC_{50} when combined, emphasizing the potent impact of this combination.

Evaluating the effects of the therapeutic agents on HeLa cells with GBS exposure. Based on the promising therapeutic effects observed, we hypothesized that these anticancer agents (binimetinib, ridaforolimus and their combination) might affect HeLa cells exposed to GBS more than the group of cells without exposure to GBS. Experiments were conducted to confirm this hypothesis.

After 6 h of exposure of HeLa cells to GBS, the cells were treated with therapeutic agents (monotherapy and combination therapy). As shown in Fig. S5A, both monotherapies and combination therapies exhibited enhanced effects on HeLa cells exposed to GBS compared with the control group after 24 h of treatment, with the combination therapy demonstrating a more pronounced effect than monotherapy.

In addition, the data specifically indicated that combination therapy was more effective in HeLa cells exposed to GBS than in those not exposed to GBS (Fig. S5B).

Discussion

Numerous studies have suggested that *Streptococcus* may be involved in cancer initiation, progression and metastasis. For instance, *Streptococcus anginosus* has been associated with activating gastric tumorigenesis (54). *Streptococcus gallolyticus subsp. Gallolyticus* is strongly linked to promoting human colon cancer cell proliferation by increasing β-catenin signaling (55). Similarly, *Streptococcus pneumoniae* is related to upregulated mTOR2/AKT signaling pathways for invasion and migration in lung cancer cells (56). Despite these observations, the understanding of the interaction between *Streptococcus* and CC remains limited. Therefore, the present study aimed to elucidate the underlying mechanism of this interaction, with a specific focus on the relationship between GBS and AC. The selection of GBS for the present study was based on its prevalence as a Gram-positive coccus, often carried asymptomatically by numerous women (57). Furthermore, it has been reported to be associated with various types of CIN in CC (19,20). Regarding the CC subtype selection, AC was chosen due to its poor prognosis compared with SCC (3). Notably, treatment strategies for AC lack specificity in clinical settings (58,59), adding significance to the present investigation.

The comprehensive transcriptomic analysis using *in vivo* public data (TCGA-CESC) and *in vitro* time series data revealed that the 'MAPK signaling pathway' and 'mTORC1 signaling' emerged as crucial elements in the host-GBS interaction.

Elevated MAPK pathway activation is implicated in cancer occurrence and progression, making it a pertinent target for investigation (60,61). Research also indicates that pathogens often target host signaling pathways to regulate a number of cell processes in cancer, and the most common pathway observed is MAPK signaling (62). Among the MAPK cascades, ERK1/2 is particularly noted for its role in regulating cell proliferation, survival, metabolism, migration and differentiation (63,64), while p38 is more closely associated with stress responses and inflammation (65). Nevertheless, the present study revealed that the interaction between GBS and HeLa cells involved MAPK signaling via ERK1/2, serving a more dominant role than the p38 pathway.

The activation of mTORC1 pathways was confirmed by the upregulation of p-AKT and p-mTOR in HeLa cells exposed to GBS for 24 h, as demonstrated by western blot analysis. The activated p-AKT Ser473 can phosphorylate and inhibit TSC complex subunit 2 (TSC2), a negative regulator of mTORC1. The inhibition of TSC2 leads to the activation of the Rheb GTPase, which in turn directly activates the mTORC1 signaling pathway (66,67). This pathway serves a crucial role in various cellular processes, including cell viability, proliferation and metabolism (68,69). Dysregulation of mTORC1 signaling has been implicated in the development and progression of cancer (66-68).

The present study also validated the expression of genes related to the MAPK pathway (FGF21, NGF, IL1A and IL1B) and the mTORC1 pathway (DDIT3, CTH, ASNS and NUPR1) from cluster 2 using RT-qPCR. Most of these genes were upregulated in HeLa cells exposed to GBS for 24 h compared with control cells at 24 h. Previous studies have shown that these genes are associated with enhancement of MAPK and mTORC1 pathway activation (70-77), as well as cancer cell progression and proliferation (78-84).

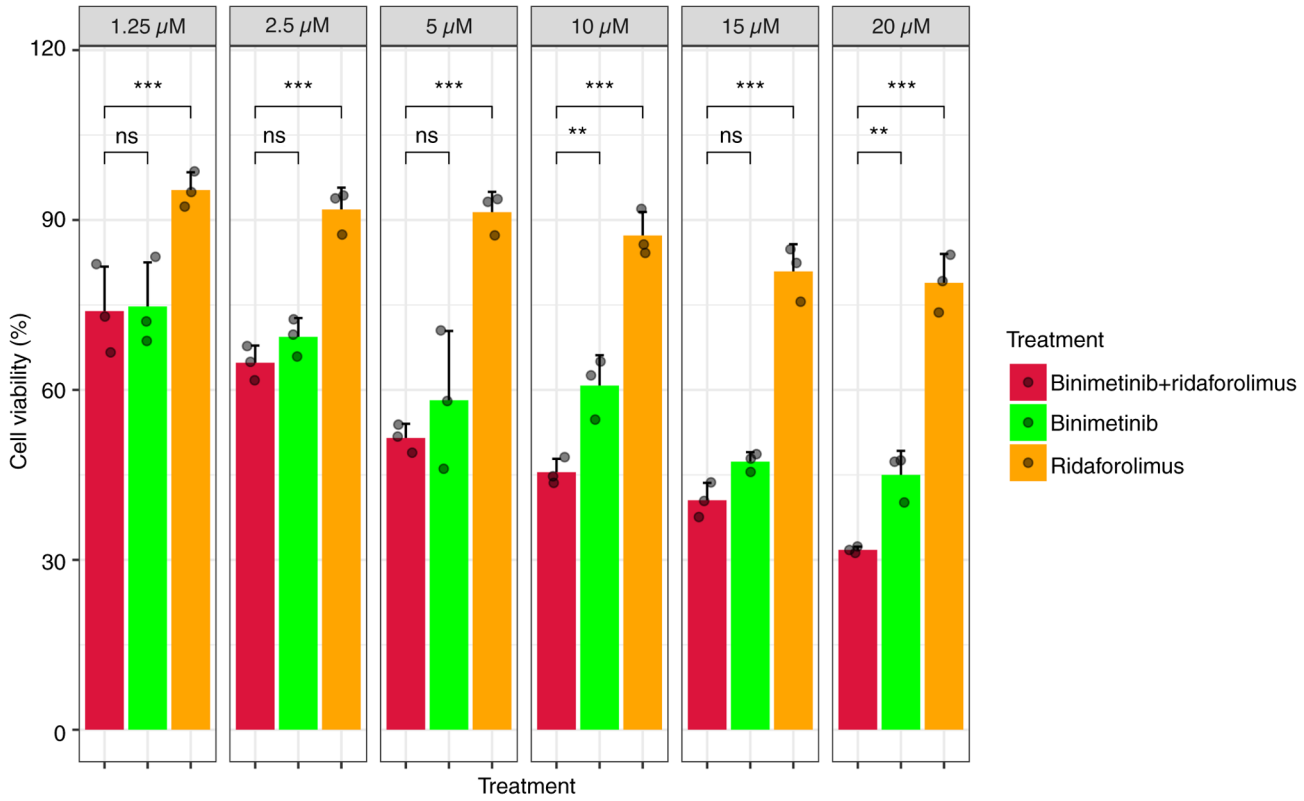

Figure 11. Comparison of MTS assay results between monotherapies and combination therapy in HeLa cells after 48 h. Green, orange and red represent the cell viability percentages for the binimetinib, ridaforolimus and combination (binimetinib + ridaforolimus) groups, respectively. **P<0.01, ***P<0.001. ns, not significant.

To evaluate the association between cell proliferation and GBS, HeLa cells were examined after exposure to GBS for 6-24 h. A significant decrease in HeLa cell numbers was observed after 6 h of GBS exposure, indicating an initial cytotoxic effect. This phenomenon was similar to the results of a study by Tyrrell *et al* (85), which examined cell death at 6 h of direct contact between HeLa cells and GBS. However, after 6 h of exposure, the number of viable cells increased and reached levels similar to the control cells at 24 h. This phenomenon was confirmed by elevated Ki67 expression, a common cell proliferation marker, present during the active phases of the cell cycle (G_1, S, G_2 and M) and absent in resting cells (G_0) (86,87). Ki67 expression was significantly higher in GBS-treated HeLa cells at 6 and 24 h compared with that in control cells, indicating that GBS treatment stimulated cell proliferation. The peak in Ki67 expression at 6 h may reflect a rapid initiation of cell cycle activity, with numerous cells entering or actively progressing through the cycle. Since Ki67 levels typically peak at G_2 or during the mitosis phase (88), the subsequent decrease at 24 h could suggest that fewer cells were entering the cell cycle or that cells that initially proliferated had completed division, resulting in a lower Ki67 signal at this time point.

According to Burnham *et al* (89), GBS could protect HeLa cells from caspase-3-induced apoptosis during early exposure by triggering the PI3K/AKT signaling pathway. Since mTORC1 signaling is a subsequent cascade of PI3K/AKT, the present results contributed to understanding the complex mechanisms underlying the interaction between HeLa cells and GBS more comprehensively than before.

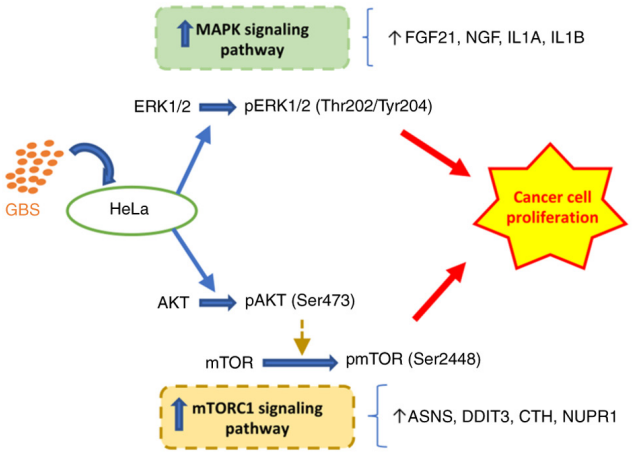

Figure 12. Schematic diagram of GBS-induced HeLa cell proliferation via MAPK and mTOR pathway activation. ASNS, asparagine synthetase (glutamine-hydrolyzing); CTH, cystathionine γ-lyase; DDIT3, DNA damage inducible transcript 3; FGF21, fibroblast growth factor 21; GBS, group B *Streptococcus*; NGF, nerve growth factor; NUPR1, nuclear protein 1; p, phosphorylated.

In general, while GBS may initially cause cell stress or death, it subsequently activates survival and proliferative pathways, specifically the MAPK and mTORC1 pathways, leading to the recovery and proliferation of HeLa cells (Fig. 12).

While several signaling pathways, such as the ERK/MAPK, PI3K/AKT, EGFR/VEGF and Wnt signaling pathways, are activated in CC development, evidence for specific pathways in AC is limited (24,90,91). By highlighting the importance of MAPK and mTORC1 signaling pathways in the interplay between AC cells and GBS, the present study provided indirect evidence of their crucial role in AC development mechanisms. Furthermore, building upon this observation, a promising therapeutic approach for AC may be targeting these signaling pathways through a drug repositioning strategy.

Drug repurposing refers to the process of identifying novel uses for existing drugs that were initially developed for a different therapeutic indication (92,93). This can potentially reduce the time and costs associated with drug development. In alignment with this strategy, the present study investigated the MEK inhibitor binimetinib and the mTOR inhibitor ridaforolimus, which were initially developed for the treatment of other cancer types (94-97) but have not been previously studied in the context of AC therapy.

While binimetinib showed a modest cytotoxic effect, it demonstrated a significant cytostatic impact on HeLa cells after 48 h, as indicated by a decrease in the absorbance at 490 nm compared with the control group in the MTS assay. The cytostatic effect refers to its ability to inhibit or slow down the viability and proliferation of cancer cells, providing a means of controlling cancer progression (98). Conversely, ridaforolimus exhibited limited efficacy in achieving the desired IC_{50} level after 48 h, accompanied by mild cytotoxic effects. These findings prompted further investigation into strategies to enhance the effectiveness of both binimetinib and ridaforolimus.

Evidence suggests the efficacy of mTOR inhibitors, such as rapamycin and its analogs, in cancer treatment (66,99). However, the development of resistance poses a challenge to their long-term effectiveness (100). Targeted inhibition of mTOR can induce MAPK reactivation and lead to resistance to single mTOR inhibition (24,101). To address this challenge, a combinatorial approach targeting mTOR and MAPK signaling should be considered for a more effective response to therapies (102,103). Accordingly, a combination study involving binimetinib and ridaforolimus was conducted. Despite the synergy score suggesting an additive effect, the MTS and apoptosis assays revealed that the combination outperformed using binimetinib or ridaforolimus alone by significantly inhibiting cell proliferation at the concentrations of 10 and 20 μM and exhibiting a robust cytotoxic effect. This outcome underscored the importance of exploring combination therapies, as they may yield more effective results than monotherapy treatments in AC. In particular, the combination (binimetinib and ridaforolimus) was more effective in the group of HeLa cells with GBS exposure than in the group without exposure. This indicated the important role of this combination in treating patients with AC with GBS dominant in their microbiome profile.

A limitation of the present study is the absence of *in vivo* experiments, which restricts the ability to fully understand the physiological relevance and systemic impact of MAPK and mTORC1 pathway activation in response to GBS exposure. Future *in vivo* studies are needed to validate the findings and assess their implications in a more complex biological context, as well as to assess the potential efficacy and safety of these drugs for AC management.

In conclusion, the present transcriptomic analysis revealed the complex molecular interaction between GBS and AC, highlighting the crucial involvement of the 'MAPK signaling pathway' and 'mTORC1 signaling'. The combination of two anticancer drugs targeting these pathways, binimetinib and ridaforolimus, might become a potential therapy for the treatment of AC, offering a promising direction for future research and clinical investigation.

Acknowledgements

Not applicable.

Funding

This research was supported by the Brain Pool program funded by the Ministry of Science and ICT through the National Research Foundation of Korea (grant no. RS-2023-00283791).

Availability of data and materials

The RNA sequencing data have been deposited in the National Center for Biotechnology Information Gene Expression Omnibus database under accession number GSE264492 or at the following URL: https://www.ncbi.nlm.nih.gov/geo/query/acc.cgi?acc=GSE264492. All other data generated in the present study may be requested from the corresponding author.

Authors' contributions

HSH and JHS were responsible for study conception. HSH, JHS, HDTN and TML were responsible for study design. HDTN, TML, YC, DL, DRJ and YJ performed the experiments. HDTN, TML, DL and HSH analyzed the data. HDTN wrote the original draft. IS, JC, NJYP, GOC, YC, OEL, YJ and DRJ contributed to data interpretation and revised the manuscript. HDTN and TML confirm the authenticity of all the raw data. All authors have read and approved the final manuscript.

Ethics approval and consent to participate

Not applicable.

Patient consent for publication

Not applicable.

Competing interests

The authors declare that they have no competing interests.

Reference

1. Sung H, Ferlay J, Siegel RL, Laversanne M, Soerjomataram I, Jemal A and Bray F: Global cancer statistics 2020: GLOBOCAN estimates of incidence and mortality worldwide for 36 cancers in 185 countries. CA Cancer J Clin 71: 209-249, 2021.
2. Burmeister CA, Khan SF, Schäfer G, Mbatani N, Adams T, Moodley J and Prince S: Cervical cancer therapies: Current challenges and future perspectives. Tumour Virus Res 13: 200238, 2022.

3. Couvreur K, Naert E, De Jaeghere E, Tummers P, Makar A, De Visschere P, Van Bockstal M, Van Dorpe J, De Neve W, Denys H and Vandecasteele K: Neo-adjuvant treatment of adenocarcinoma and squamous cell carcinoma of the cervix results in significantly different pathological complete response rates. BMC Cancer 18: 1101, 2018.
4. Blake SJ, Wolf Y, Boursi B and Lynn DJ: Role of the microbiota in response to and recovery from cancer therapy. Nat Rev Immunol 24: 308-325, 2024.
5. Sun J, Chen F and Wu G: Potential effects of gut microbiota on host cancers: Focus on immunity, DNA damage, cellular pathways, and anticancer therapy. ISME J 17: 1535-1551, 2023.
6. Wu S, Ding X, Kong Y, Acharya S, Wu H, Huang C, Liang Y, Nong X and Chen H: The feature of cervical microbiota associated with the progression of cervical cancer among reproductive females. Gynecol Oncol 163: 348-357, 2021.
7. Tango CN, Seo SS, Kwon M, Lee DO, Chang HK and Kim MK: Taxonomic and functional differences in cervical microbiome associated with cervical cancer development. Sci Rep 10: 9720, 2020.
8. Xu X, Zhang Y, Yu L, Shi X, Min M, Xiong L, Pan J, Liu P, Wu G and Gao G: A cross-sectional analysis about bacterial vaginosis, high-risk human papillomavirus infection, and cervical intraepithelial neoplasia in Chinese women. Sci Rep 12: 6609, 2022.
9. Audirac-Chalifour A, Torres-Poveda K, Bahena-Román M, Téllez-Sosa J, Martínez-Barnetche J, Cortina-Ceballos B, López-Estrada G, Delgado-Romero K, Burguete-García AI, Cantú D, *et al*: Cervical microbiome and cytokine profile at various stages of cervical cancer: A pilot study. PLoS One 11: e0153274, 2016.
10. Nguyen HDT, Le TM, Lee E, Lee D, Choi Y, Cho J, Park NJ, Chong GO, Seo I and Han HS: Relationship between human papillomavirus status and the cervicovaginal microbiome in cervical cancer. Microorganisms 11: 1417, 2023.
11. Hu J, Wu Y, Quan L, Yang W, Lang J, Tian G and Meng B: Research of cervical microbiota alterations with human papillomavirus infection status and women age in Sanmenxia area of China. Front Microbiol 13: 1004664, 2022.
12. Mulato-Briones IB, Rodriguez-Ildefonso IO, Jiménez-Tenorio JA, Cauich-Sánchez PI, Méndez-Tovar MDS, Aparicio-Ozores G, Bautista-Hernández MY, González-Parra JF, Cruz-Hernández J, López-Romero R, *et al*: Cultivable microbiome approach applied to cervical cancer exploration. Cancers (Basel) 16: 314, 2024.
13. Kang GU, Jung DR, Lee YH, Jeon SY, Han HS, Chong GO and Shin JH: Potential association between vaginal microbiota and cervical carcinogenesis in korean women: A cohort study. Microorganisms 294: 294, 2021.
14. Armistead B, Oler E, Adams Waldorf K and Rajagopal L: The double life of Group B streptococcus: Asymptomatic colonizer and potent pathogen. J Mol Biol 431: 2914-2931, 2019.
15. Aksu B and Yanilmaz O: Group B streptococci induce interleukin 8 production in human cervical epithelial cell cultures: The role of capsule polysaccharide. Clin Exp Health Sci 9: 49-52, 2018.
16. Maisey HC, Doran KS and Nizet V: Recent advances in understanding the molecular basis of group B Streptococcus virulence. Expert Rev Mol Med 10: e27, 2008.
17. Patras KA, Rösler B, Thoman ML and Doran KS: Characterization of host immunity during persistent vaginal colonization by Group B Streptococcus. Mucosal Immunol 8: 1339-1348, 2015.
18. Patras KA, Wang NY, Fletcher EM, Cavaco CK, Jimenez A, Garg M, Fierer J, Sheen TR, Rajagopal L and Doran KS: Group B Streptococcus CovR regulation modulates host immune signalling pathways to promote vaginal colonization. Cell Microbiol 15: 1154-1167, 2013.
19. Zhang C, Liu Y, Gao W, Pan Y, Gao Y, Shen J and Xiong H: The direct and indirect association of cervical microbiota with the risk of cervical intraepithelial neoplasia. Cancer Med 7: 2172-2179, 2018.
20. Lee YH, Kang GU, Jeon SY, Tagele SB, Pham HQ, Kim MS, Ahmad S, Jung DR, Park YJ, Han HS, *et al*: Vaginal microbiome-based bacterial signatures for predicting the severity of cervical intraepithelial neoplasia. Diagnostics (Basel) 10: 1013, 2020.
21. Mutz KO, Heilkenbrinker A, Lönne M, Walter JG and Stahl F: Transcriptome analysis using Next-generation sequencing. Curr Opin Biotechnol 24: 22-30, 2013.
22. Ahmed W: RNA-seq resolving host-pathogen interactions: Advances and applications. Ecol Genet Genom 15: 100057, 2020.
23. Nathan S: Transcriptome profiling to understand Host-bacteria interactions: Past, present and future. ScienceAsia 46: 503-513, 2020.
24. Yip HYK and Papa A: Signaling pathways in cancer: Therapeutic targets, combinatorial treatments, and new developments. Cells 10: 659, 2021.
25. Kwon OS, Kim W, Cha HJ and Lee H: In silico drug repositioning: From Large-scale transcriptome data to therapeutics. Arch Pharm Res 42: 879-889, 2019.
26. Poore GD, Kopylova E, Zhu Q, Carpenter C, Fraraccio S, Wandro S, Kosciolek T, Janssen S, Metcalf J, Song SJ, *et al*: Microbiome analyses of blood and tissues suggest cancer diagnostic approach. Nature 579: 567-574, 2020.
27. Love MI, Huber W and Anders S: Moderated estimation of fold change and dispersion for RNA-seq data with DESeq2. Genome Biol 15: 550, 2014.
28. Zhang B and Horvath S: A general framework for weighted gene co-expression network analysis. Stat Appl Genet Mol Biol 4: 17, 2005.
29. Langfelder P and Horvath S: WGCNA: An R package for weighted correlation network analysis. BMC Bioinformatics 9: 559, 2008.
30. Kolberg L, Raudvere U, Kuzmin I, Adler P, Vilo J and Peterson H: g:Profiler-interoperable web service for functional enrichment analysis and gene identifier mapping (2023 update). Nucleic Acids Res 51: W207-W212, 2023.
31. Kuleshov MV, Jones MR, Rouillard AD, Fernandez NF, Duan Q, Wang Z, Koplev S, Jenkins SL, Jagodnik KM, Lachmann A, *et al*: Enrichr: A comprehensive gene set enrichment analysis web server 2016 update. Nucleic Acids Res 44: W90-W97, 2016.
32. Kanehisa M and Goto S: KEGG: Kyoto encyclopedia of genes and genomes. Nucleic Acids Res 28: 27-30, 2000.
33. Liberzon A, Birger C, Thorvaldsdóttir H, Ghandi M, Mesirov JP and Tamayo P: The molecular signatures database hallmark gene set collection. Cell Syst 1: 417-425, 2015.
34. Wickham H: ggplot2: Elegant graphics for data analysis. second edition. Springer-Verlag New York, 2016.
35. Ewels P, Magnusson M, Lundin S and Käller M: MultiQC: Summarize analysis results for multiple tools and samples in a single report. Bioinformatics 32: 3047-3048, 2016.
36. Andrews S: FastQC: A Quality Control Tool for High Throughput Sequence Data., 2010.
37. Martin M: Cutadapt Removes Adapter Sequences From High-Throughput Sequencing Reads., 2011.
38. Dobin A, Davis CA, Schlesinger F, Drenkow J, Zaleski C, Jha S, Batut P, Chaisson M and Gingeras TR: STAR: Ultrafast universal RNA-seq aligner. Bioinformatics 29: 15-21, 2013.
39. Lefol Y, Korfage T, Mjelle R, Prebensen C, Lüders T, Müller B, Krokan H, Sarno A, Alsøe L; CONSORTIUM LEMONAID, *et al*: TiSA: TimeSeriesAnalysis-A pipeline for the analysis of longitudinal transcriptomics data. NAR Genom Bioinform 5: lqad020, 2023.
40. Nilsen G, Borgan Ø, LiestØl K and Lingjærde OC: Identifying clusters in genomics data by recursive partitioning. Stat Appl Genet Mol Biol 12: 637-652, 2013.
41. Livak KJ and Schmittgen TD: Analysis of relative gene expression data using real-time quantitative PCR and the 2(-Delta Delta C(T)) method. Methods 25: 402-408, 2001.
42. Lamb J, Crawford ED, Peck D, Modell JW, Blat IC, Wrobel MJ, Lerner J, Brunet JP, Subramanian A, Ross KN, *et al*: The connectivity map: Using gene-expression signatures to connect small molecules, genes, and disease. Science 313: 1929-1935, 2006.
43. Samart K, Tuyishime P, Krishnan A and Ravi J: Reconciling multiple connectivity scores for drug repurposing. Brief Bioinform 22: bbab161, 2021.
44. Subramanian A, Narayan R, Corsello SM, Peck DD, Natoli TE, Lu X, Gould J, Davis JF, Tubelli AA, Asiedu JK, *et al*: A next generation connectivity map: L1000 platform and the first 1,000,000 profiles. Cell 171: 1437-1452.e17, 2017.
45. Ritz C, Baty F, Streibig JC and Gerhard D: Dose-response analysis using R. PLoS One 10: e0146021, 2015.
46. Zheng S, Wang W, Aldahdooh J, Malyutina A, Shadbahr T, Tanoli Z, Pessia A and Tang J SynergyFinder plus: Toward better interpretation and annotation of drug combination screening datasets. Genomics Proteomics Bioinformatics 20: 587-596, 2022.
47. Xia T, Xu LL, Guo PY, Shi WT, Cheng YQ and Liu AJ: Synergism of amlodipine and telmisartan or candesartan on blood pressure reduction by using SynergyFinder 3.0 and probability sum test in vivo. Pharmacol Res Perspect 11: e01064, 2023.

48. Holm S: A simple sequentially rejective multiple test procedure a simple sequentially rejective multiple test procedure. Stat Medics 6: 65-70, 1979.
49. Zhang Y, Zhang Y, Li M, Meng F, Yu Z, Chen Y and Cui G: Combination of SB431542, CHIR99021 and PD0325901 has a synergic effect on abrogating valproic acid-induced epithelial-mesenchymal transition and stemness in HeLa, 5637 and SCC-15 cells. Oncol Rep 41: 3545-3554, 2019.
50. Ye H, Zhang Y, Wang Y, Xia J, Mao X and Yu X: The restraining effect of baicalein and U0126 on human cervical cancer cell line HeLa. Mol Med Rep 16: 957-963, 2017.
51. Yang EJ and Chang JH: PD98059 induces the apoptosis of human cervical cancer cells by regulating the expression of Bcl2 and ERK2. J Exp Biomed Sci 17: 291-295, 2011.
52. Zahmatyar M, Kharaz L, Abiri Jahromi N, Jahanian A, Shokri P and Nejadghaderi SA: The safety and efficacy of binimetinib for lung cancer: A systematic review. BMC Pulm Med 24: 379, 2024.
53. Tran B and Cohen MS: The discovery and development of binimetinib for the treatment of melanoma. Expert Opin Drug Discov 15: 745-754, 2020.
54. Fu K, Cheung AHK, Wong CC, Liu W, Zhou Y, Wang F, Huang P, Yuan K, Coker OO, Pan Y, *et al*: *Streptococcus anginosus* promotes gastric inflammation, atrophy, and tumorigenesis in mice. Cell 187: 882-896, 2024.
55. Kumar R, Herold JL, Schady D, Davis J, Kopetz S, Martinez-Moczygemba M, Murray BE, Han F, Li Y, Callaway E, *et al*: *Streptococcus gallolyticus* subsp. gallolyticus promotes colorectal tumor development. PLoS Pathog 13: e1006440, 2017.
56. Song X, Liu B, Zhao G, Pu X, Liu B, Ding M and Xue Y: *Streptococcus pneumoniae* promotes migration and invasion of A549 cells in vitro by activating mTORC2/AKT through up-regulation of DDIT4 expression. Front Microbiol 13: 1046226, 2022.
57. Choi Y, Han HS, Chong GO, Le TM, Nguyen HDT, Lee OE, Lee D, Seong WJ, Seo I and Cha HH: Updates on Group B streptococcus infection in the field of obstetrics and gynecology. Microorganisms 10: 2398, 2022.
58. Hsieh HY, Lu CH and Wang L: Long-term treatment outcomes/toxicities of definite chemoradiotherapy (intensity-modulated radiation therapy) for early-stage 'bulky' cervical cancer and survival impact of histological subtype. J Formos Med Assoc 122: 221-229, 2023.
59. Pan X, Yang W, Wen Z, Li F, Tong L and Tang W: Does adenocarcinoma have a worse prognosis than squamous cell carcinoma in patients with cervical cancer? A real-world study with a propensity score matching analysis. J Gynecol Oncol 31: e80, 2020.
60. Guo Y, Pan W, Liu S, Shen Z, Xu Y and Hu L: ERK/MAPK signalling pathway and tumorigenesis (Review). Exp Ther Med 19: 1997-2007, 2020.
61. Burotto M, Chiou VL, Lee JM and Kohn EC: The MAPK pathway across different malignancies: A new perspective. Cancer 120: 3446-3456, 2014.
62. Alto NM and Orth K: Subversion of cell signaling by pathogens. Cold Spring Harb Perspect Biol 4: a006114, 2012.
63. Guo Y, Pan W, Liu S, Shen Z, Xu Y and Hu L: ERK/MAPK signalling pathway and tumorigenesis. Exp Ther Med 19: 1997-2007, 2020.
64. Lavoie H, Gagnon J and Therrien M: ERK signalling: A master regulator of cell behaviour, life and fate. Nat Rev Mol Cell Biol 21: 607-632, 2020.
65. Raingeaud J, Gupta S, Rogers JS, Dickens M, Han J, Ulevitch RJ and Davis RJ: Pro-inflammatory cytokines and environmental stress cause p38 mitogen-activated protein kinase activation by dual phosphorylation on tyrosine and threonine. J Biol Chem 270: 7420-7426, 1995.
66. Tian T, Li X and Zhang J: mTOR signaling in cancer and mtor inhibitors in solid tumor targeting therapy. Int J Mol Sci 20: 755, 2019.
67. Zou Z, Tao T, Li H and Zhu X: MTOR signaling pathway and mTOR inhibitors in cancer: Progress and challenges. Cell Biosci 10: 31, 2020.
68. Ben-Sahra I and Manning BD: mTORC1 signaling and the metabolic control of cell growth. Curr Opin Cell Biol 45: 72-82, 2017.
69. Pópulo H, Lopes JM and Soares P: The mTOR signalling pathway in human cancer. Int J Mol Sci 13: 1886-1918, 2012.
70. Fisher FM and Maratos-Flier E: Understanding the physiology of FGF21. Annu Rev Physiol 78: 223-241, 2016.
71. Meng D, Yang Q, Wang H, Melick CH, Navlani R, Frank AR and Jewell JL: Glutamine and asparagine activate mTORC1 independently of Rag GTPases. J Biol Chem 295: 2890-2899, 2020.
72. Gobert AP, Latour YL, Asim M, Finley JL, Verriere TG, Barry DP, Milne GL, Luis PB, Schneider C, Rivera ES, *et al*: Bacterial pathogens hijack the innate immune response by activation of the reverse transsulfuration pathway. mBio 10: e02174-19, 2019.
73. Xing J, Kornhauser JM, Xia Z, Thiele EA and Greenberg ME: Nerve growth factor activates extracellular Signal-regulated kinase and p38 Mitogen-activated protein kinase pathways to stimulate CREB serine 133 Phosphorylation. Mol Cell Biol 18: 1946-1955, 1998.
74. Yang HT, Cohen P and Rousseau S: IL-1β-stimulated activation of ERK1/2 and p38α MAPK mediates the transcriptional up-regulation of IL-6, IL-8 and GRO-α in HeLa cells. Cell Signal 20: 375-380, 2008.
75. Li S, Deng P, Wang M, Liu X, Jiang M, Jiang B, Yang L and Hu J: IL-1α and IL-1β promote NOD2-induced immune responses by enhancing MAPK signaling. Lab Invest 99: 1321-1334, 2019.
76. Liu W, Feng Z, Qu N, Li R and Niu Y: NUPR1 contribution to autophagy in primary bone tumor cells by regulating the AKT/mTOR signaling pathway. Acta Medica Mediterranea 38: 1223-1228, 2022.
77. Yang C, Xu X, Dong X, Yang B, Dong W, Luo Y, Liu X, Wu Y and Wang J: DDIT3/CHOP promotes autophagy in chondrocytes via SIRT1-AKT pathway. Biochim Biophys Acta Mol Cell Res 1868: 119074, 2021.
78. Fan T, Wang X, Zhang S, Deng P, Jiang Y, Liang Y, Jie S, Wang Q, Li C, Tian G, *et al*: NUPR1 promotes the proliferation and metastasis of oral squamous cell carcinoma cells by activating TFE3-dependent autophagy. Signal Transduct Target Ther 7: 130, 2022.
79. Wang Y, Huang J, Chen W, Wang RH, Kao MC, Pan YR, Chan SH, Tsai KW, Kung HJ, Lin KT and Wang LH: Dysregulation of cystathionine γ-lyase promotes prostate cancer progression and metastasis. EMBO Rep 20: e45986, 2019.
80. Lin H, Liu S, Gao W and Liu H: DDIT3 modulates cancer stemness in gastric cancer by directly regulating CEBPβ. J Pharm Pharmacol 72: 807-815, 2020.
81. Krall AS, Xu S, Graeber TG, Braas D and Christofk HR: Asparagine promotes cancer cell proliferation through use as an amino acid exchange factor. Nat Commun 7: 11457, 2016.
82. Gelfo V, Romaniello D, Mazzeschi M, Sgarzi M, Grilli G, Morselli A, Manzan B, Rihawi K and Lauriola M: Roles of il-1 in cancer: From tumor progression to resistance to targeted therapies. Int J Mol Sci 21: 6009, 2020.
83. Molloy NH, Read DE and Gorman AM: Nerve growth factor in cancer cell death and survival. Cancers (Basel) 3: 510-530, 2011.
84. Sui Y, Liu Q, Xu C, Ganesan K, Ye Z, Li Y, Wu J, Du B, Gao F, Song C and Chen J: Non-alcoholic fatty liver disease promotes breast cancer progression through upregulated hepatic fibroblast growth factor 21. Cell Death Dis 15: 67, 2024.
85. Tyrrell GJ, Kennedy A, Shokoples SE and Sherburne RK: Binding and invasion of HeLa and MRC-5 cells by *Streptococcus agalactiae*. Microbiology (Reading) 148: 3921-3931, 2002.
86. Gerdes J, Lemke H, Baisch H, Wacker H, Schwab U and Stein H: Cell cycle analysis of a cell proliferation-associated human nuclear antigen defined by the monoclonal antibody Ki-67. J Immunol 133: 1710-1715, 1984.
87. Schlfiter C, Duchrow M, Wohlenberg C, Becker MHG, Key G, Flad HD and Gerdes J: The cell Proliferation-associated antigen of antibody Ki-67: A very large, ubiquitous nuclear protein with numerous repeated elements, representing a new kind of cell cycle-maintaining proteins. J Cell Biol 123: 513-522, 1993.
88. Uxa S, Castillo-Binder P, Kohler R, Stangner K, Müller GA and Engeland K: Ki-67 gene expression. Cell Death Differ 28: 3357-3370, 2021.
89. Burnham CAD, Shokoples SE and Tyrrell GJ: Invasion of HeLa cells by group B streptococcus requires the phosphoinositide-3-kinase signalling pathway and modulates phosphorylation of host-cell Akt and glycogen synthase kinase-3. Microbiology (Reading) 153: 4240-4252, 2007.
90. Ji J and Zheng PS: Activation of mTOR signaling pathway contributes to survival of cervical cancer cells. Gynecol Oncol 117: 103-108, 2010.
91. Li XW, Tuergan M and Abulizi G: Expression of MAPK1 in cervical cancer and effect of MAPK1 gene silencing on epithelial-mesenchymal transition, invasion and metastasis. Asian Pac J Trop Med 8: 937-943, 2015.

92. Weth FR, Hoggarth GB, Weth AF, Paterson E, White MPJ, Tan ST, Peng L and Gray C: Unlocking hidden potential: Advancements, approaches, and obstacles in repurposing drugs for cancer therapy. Br J Cancer 130: 703-715, 2023.
93. K W To K and Cho WCS: Drug repurposing for cancer therapy in the era of precision medicine. Curr Mol Pharmacol 15: 895-903, 2022.
94. Colombo N, McMeekin DS, Schwartz PE, Sessa C, Gehrig PA, Holloway R, Braly P, Matei D, Morosky A, Dodion PF, *et al*: Ridaforolimus as a single agent in advanced endometrial cancer: Results of a single-arm, phase 2 trial. Br J Cancer 108: 1021-1026, 2013.
95. Chon HS, Kang S, Lee JK, Apte SM, Shahzad MM, Williams-Elson I and Wenham RM: Phase I study of oral ridaforolimus in combination with paclitaxel and carboplatin in patients with solid tumor cancers. BMC Cancer 17: 407, 2017.
96. Finn RS, Ahn DH, Javle MM, Tan BR Jr, Weekes CD, Bendell JC, Patnaik A, Khan GN, Laheru D, Chavira R, *et al*: Phase 1b investigation of the MEK inhibitor binimetinib in patients with advanced or metastatic biliary tract cancer. Invest New Drugs 36: 1037-1043, 2018.
97. Woodfield SE, Zhang L, Scorsone KA, Liu Y and Zage PE: Binimetinib inhibits MEK and is effective against neuroblastoma tumor cells with low NF1 expression. BMC Cancer 16L: 172, 2016.
98. Anttila JV, Shubin M, Cairns J, Borse F, Guo Q, Mononen T, Vázquez-García I, Pulkkinen O and Mustonen V: Contrasting the impact of cytotoxic and cytostatic drug therapies on tumour progression. PLoS Comput Biol 15: e1007493, 2019.
99. Hua H, Kong Q, Zhang H, Wang J, Luo T and Jiang Y: Targeting mTOR for cancer therapy. J Hematol Oncol 12: 71, 2019.
100. Formisano L, Napolitano F, Rosa R, D'Amato V, Servetto A, Marciano R, De Placido P, Bianco C and Bianco R: Mechanisms of resistance to mTOR inhibitors. Crit Rev Oncol Hematol 147: 102886, 2020.
101. Carracedo A, Ma L, Teruya-Feldstein J, Rojo F, Salmena L, Alimonti A, Egia A, Sasaki AT, Thomas G, Kozma SC, *et al*: Inhibition of mTORC1 leads to MAPK pathway activation through a PI3K-dependent feedback loop in human cancer. J Clin Invest 118: 3065-3074, 2008.
102. Li Q, Li Z, Luo T and Shi H: Targeting the PI3K/AKT/mTOR and RAF/MEK/ERK pathways for cancer therapy. Mol Biomed 3: 47, 2022.
103. Pitts TM, Newton TP, Bradshaw-Pierce EL, Addison R, Arcaroli JJ, Klauck PJ, Bagby SM, Hyatt SL, Purkey A, Tentler JJ, *et al*: Dual pharmacological targeting of the map kinase and pi3k/mtor pathway in preclinical models of colorectal cancer. PLoS One 9: e113037, 2014.

Copyright © 2024 Nguyen et al. This work is licensed under a Creative Commons Attribution-NonCommercial-NoDerivatives 4.0 International (CC BY-NC-ND 4.0) License.